WWW.IJRPR.COM

International Journal of Research Publication and Reviews

Journal homepage: www.ijrpr.com ISSN 2582-7421

Review on Droop Controller for Power and Current Limiting

Lovlesh Nageshwer [1]and Prof. Manish Kethoriya [2]

[1,2]Department of Electrical Engineering, School of Research and Technology, People's University, Bhopal, Madhya Pradesh, India

A B S T R A C T

Because droop control is inherently modular and simple to install, it has been used extensively in DC microgrids (MGs). Two options—I-V and V-I droop—among the several droop control strategies that can be used in DC MGs will be examined in this paper. V-I droop regulates the DC voltage based on the output current, whereas I-V droop controls the DC current based on the DC voltage. The analysis and comparison of V-I/I-V droop control strategies in MGs with an emphasis on steady-state power sharing performance and stability will be presented in this work. The associated output impedance of the source subsystem, including the dynamics of the converters, is derived by the control scheme for current-mode (I-V droop) and voltage-mode (V-I droop) systems. It also examines the stability of the power system when supplying constant power loads.

Keywords: grid-connected, distributed generation, droop controller, power and current limitation.

Introduction

Power systems stability has long been the subject of research [1]. However, the substantial integration of renewable energy sources has had a noticeable effect on the grid's ability to operate continuously and dependably in recent times [2,3]. Thus, grid-connected units now have to fulfill certain basic requirements in order to help preserve grid stability and help regulate the voltage and frequency of the grid [4]. Droop control is commonly used to guarantee stability when grid-connected inverters dominate a power system without requiring communication between the various units [5,6].

Droop Control

Droop control is a technique used in electric grids to govern inverter-based resources and synchronous generators. It enables the connection of many producing units in parallel, sharing loads in accordance with their individual power ratings. Under droop regulation, a set of frequency and voltage "droop" values are assigned to each grid generation unit. These droop values represent the allowed frequency and voltage departure from their nominal values to account for changes in power requirements [7,8].

The most used type of droop control is conventional droop control [10]. In conventional droop control, frequency and voltage change in a linear fashion with regard to active and reactive power, respectively. For instance, a converter with a 1% frequency droop will respond to a 1.0 pu change in active power by changing its frequency by 0.01 pu. Reverse droop control is another technique that can be useful in low-voltage microgrids [36].

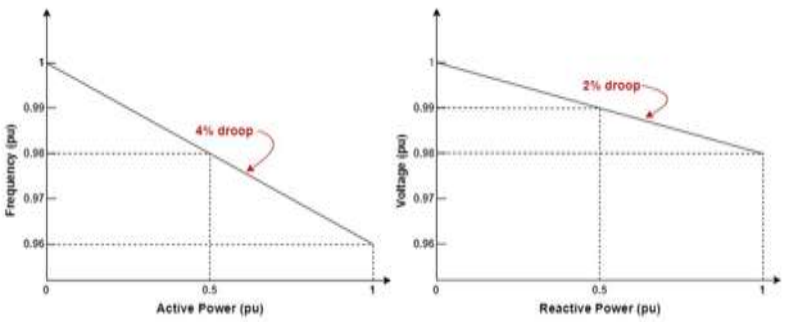

Figure 1.1 Example frequency and voltage conventional droop curves [36]

CONVENTIONAL DROOP-CONTROLS USED FOR GRID

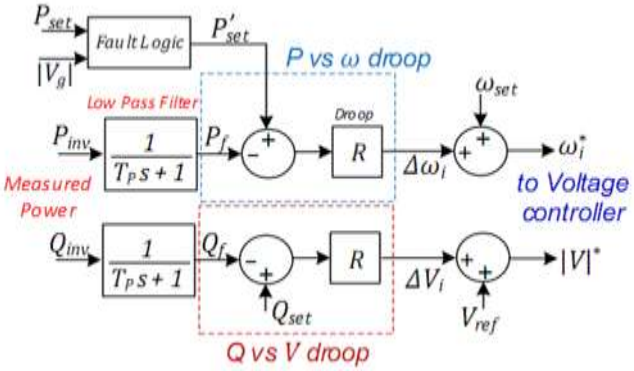

Figure 1.2 Droop control block diagram

Micro-power plants are usually interfaced with power inverters. Droop control mechanisms are installed on these inverter-interfaced distributed generators (DGs) to assist them in providing the required power to the power system to which they are linked. Droop control is usually used to increase the stability of power networks that are dominated by grid-connected inverters without any communication between the various components.

1. Droop control can be implemented in various ways, contingent on the associated impedances: P ~ ω and Q ~ V represent the droop control in the case of an inductive impedance.
2. The droop control for a resistive impedance is written as P ~ V and Q ~ −ω and,
3. P ~ −ω and Q ~ −V indicate the control of droop in the case of a capacitive impedance.

Grid-connected inverters usually have easy output current restrictions and are current-controlled; nevertheless, independent power systems with power electronics must be able to adjust voltage [16].

An example Grid-Connected Droop-Controlled Distributed Generations system with inverters acting as controllers is shown in Fig. 1.2. The internal controller regulates the voltage magnitude and frequency (ωDG) of the LCL filter capacitor at predefined reference values produced by the droop controller. In order to more effectively manipulate control variables in the DG reference frame, this controller uses the output currents of the DG as feed-forward signals. Fig. 1.2 shows the block diagram of the internal controller that is currently in use [4,18,19].

The frequency reference for distributed generation is established as:

$\omega_{ref} = \omega_0 - m_p(P - P_\theta)$ Eqn. 1.1

where P is produced by low-pass filtering of $q = \frac{3}{2} v_{od} i_{oq}$ according to

$P = \frac{\omega_c}{s+\omega_0} p$ Eqn. 1.2

In typical circumstances, when the DG injects rated active power at the Upstream Grid (UG), the reference DG frequency is ω_0, as per Eqn. (1.1). However, when the Upstream Grid frequency drops for any reason (such as an abrupt increase in the amount of active power that is demanded or a decrease in the production of power plants at the Upstream Grid), the output active power of Grid-Connected Droop-Controlled Distributed Generations begins to increase under abnormal conditions. Based on the droop characteristic (1), the DG frequency is then decreased so that the DG drawn active power is proportionate to its capacity. The DG voltage magnitude is referenced as follows:

$v_{ref} = v_0 - n_q(Q - Q_0)$ Eqn. 1.3

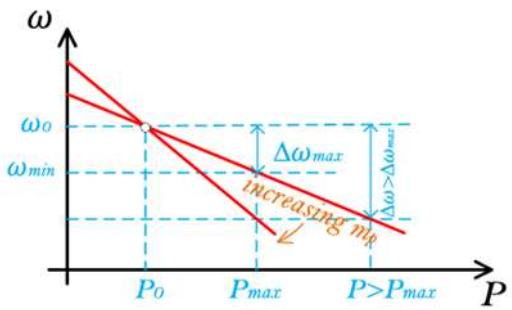

Figure 1.3 P-ω droop characteristic [4]

where Q is produced by low-pass filtering of $q = -\frac{3}{2} v_{od} i_{oq}$ according to

$Q = \frac{\omega_c}{s+\omega_0} q$ Eqn.1.4

When the DG injects rated reactive power at the UG normal conditions, Eqn. (1.3) states that v_0 is the reference of the DG volt age magnitude. However, in abnormal circumstances, the DG voltage magnitude is decreased based on the droop characteristic Eqn. (1.3) so that the DG drawn reactive power is proportionate to its capacity. This occurs when the UG voltage magnitude decreases for any reason (e.g., short circuit faults at UG), and the output reactive power of GCDCDG begins to increase.

In the above-mentioned UG situations, if the UG frequency and/or voltage magnitude drop have significant values, the output powers of the GCDCDG may exceed their maximum values. One method of limiting the output powers is to set maximum values for i_{od} and i_{oq} using current limiters.

This method restricts output reactive power in accordance with forms, however it has a problem limiting output active power. The GCDCDG frequency does not follow the UG frequency, which results in power fluctuation between DG and UG and unstable the system, as seen by the P droop characteristic (Fig. 1.3). The current limiter is saturated if the UG frequency drops and i_{od} increases. If this growing surpasses the maximum of i_{od}.

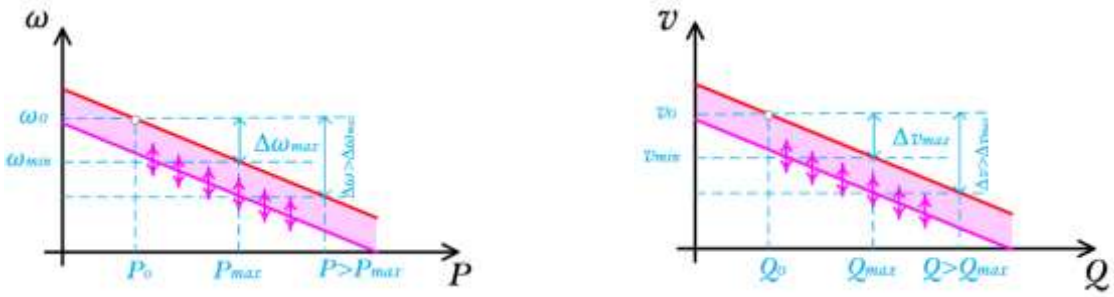

Figure 1.4 (Top) P and (bottom) Q v droop characteristic [4].

The suggested unified droop-control based current limiting technique will be explained in the following manner in order to address the aforementioned issues.

OBJECTIVE

The primary goal of this work for prepare a review report based on more than 30 papers related to the title and summarised the basic and fundamental calculations of the droop controller and systems stability.

Literature Review

A. C. Braitor et al. 2021, study for introduces a new current-limiting droop controller for parallel DC-DC boost converters in DC microgrids, ensuring stability and power sharing across various loads (constant impedance, current, or power). The controller maintains inherent current-limiting properties regardless of load type or variations, ensuring stability and accurate power sharing compared to existing methods. Simulation and experimental results validate its effectiveness [1]

A. G. Paspatis et al. 2021, proposes a novel current-limiting droop (CLD) controller for grid-connected inverters. It ensures current limitation and asymptotic stability during grid faults, maximizing power injection and providing voltage support by adjusting reactive power references. The enhanced CLD controller offers a simplified, unified control scheme for normal and faulty grid conditions, validated experimentally [2].

A. Saleh et al. 2022, addresses power and current limiting in grid-connected droop-controlled distributed generations (GCDCDGs) under fluctuations in upstream grid frequency and voltage. It proposes a new droop-control strategy that limits power and current without using traditional current limiters, maintaining stable operation. Simulations demonstrate its performance under various conditions [4].

A. Zapata et al. 2023, presents a methodology to address control challenges in power systems with high renewable energy penetration. It evaluates system stability and identifies weak points under various contingencies using transient stability and system strength assessments. The findings provide recommendations for secure interconnection of inverter-based resources in power systems [5].

Al-Saadi et al. 2021, focuses on control strategies for distributed energy storage systems (DESS), essential for transitioning to decentralized, renewable energy-based power systems. It examines centralized, decentralized, multi-agent, and intelligent control methods, emphasizing power-sharing, system resilience, and state-of-charge balancing. The review highlights recent advances and future directions in DESS control [6].

B. Mishra and M. Pattnaik 2023, proposes a modified droop-based decentralized control scheme for accurate power sharing between parallel inverters, addressing issues like impedance mismatch and frequency deviations. A virtual impedance control loop is added to enhance performance under varying conditions, validated through simulations [7].

C. Bisht and P. Kundu 2023, explores current limiting for grid-forming inverters during fault conditions. It proposes a method to reduce current reference using a d-q component current limiter, ensuring system stability and quick fault recovery. Simulations highlight the advantages of this approach under different fault scenarios [8].

C. Fang and L. Mu 2024, develops an analytical fault model for droop-controlled inverter-interfaced distributed generators (IIDGs), addressing the challenges of transient fault responses. It includes various control aspects and proposes a clustering method for IIDGs to simplify fault analysis. The model's accuracy is verified through simulations [9].

D. Celik and M. E. Meral 2019, introduces a reference current generator-based flexible power control strategy for distributed generation systems under grid faults. It minimizes power oscillations and includes current limitation for protection. Using a fractional order proportional integral controller and dual average filter phase-locked loop, the strategy is validated through theoretical analysis and simulations [10].

D. Yan et al. 2024, investigates the transient stability of grid-following (GFL) and grid-forming (GFM) inverter-based resources (IBRs) in power systems with high IBR penetration. Using a simulation model, it evaluates the performance of various GFL and GFM controllers under different conditions, such as three-phase faults and load changes. The findings highlight that GFM IBRs provide better frequency response and stability compared to GFL IBRs as penetration levels increase [11].

Dedeoglu and G. C. Konstantopoulos 2021, proposes a nonlinear droop controller for AC microgrids with parallel three-phase inverters to prevent circulating power and ensure current limiting in both stand-alone and grid-connected modes. Unlike existing methods that use saturation blocks, this controller directly limits instantaneous current values. Simulation results validate its effectiveness in maintaining stability and performance [12].

J. Liu et al. 2021, explores the regulation of DC voltage in hybrid PV and wind energy systems using the Cuttlefish Algorithm (CFA) for tuning PI controller gains. The hybrid system aims to provide uninterrupted power by leveraging the complementary nature of PV and wind energy. The CFA-tuned PI controller improves DC voltage regulation and reduces Total Harmonic Distortion (THD), as demonstrated through performance analysis [13].

L. Zhou et al. 2020, study on to enhance the low voltage ride-through (LVRT) capability of hybrid power systems using convertible static compensators (CSCs). Different CSC configurations and controller types, including Q-learning and dynamic fuzzy Q-learning (DFQL), are compared. The DFQL-based controller, particularly with UPFC and two STATCOMs, shows superior performance in improving LVRT and voltage support [15].

M. A. Awal et al. 2023, proposes a ride-through controller to maintain the grid-forming (GFM) nature of inverter-based resources (IBRs) during faults or overloads. The controller maximizes converter capacity utilization and transient stability without requiring fault detection. It addresses the limitations of existing GFM controllers, providing better performance under weak grid conditions. Experimental results confirm its effectiveness [16].

M. E. Meral and D. Çelik 2019, focuses on advanced control strategies and positive-negative sequence (PNS) extractors for distributed generation power systems (DGPSs) under normal and abnormal grid conditions. It analyzes various PNS extractors and control strategies for improving power quality and system reliability, particularly during voltage unbalances and faults. Comparative analyses highlight the effectiveness of different approaches [17].

M. E. Meral and D. Çelik 2020, proposes a proportional complex integral (PCI)-based control scheme for distributed energy inverters (DEIs) connected to the grid, addressing stability and power quality challenges. The PCI-based scheme outperforms traditional PI controllers, especially under unbalanced and distorted grid conditions, by reducing DC-link voltage oscillations and third-order current harmonics. Case studies validate the improved dynamic performance and reliability [18].

M. Eggers et al. 2020, proposes a design methodology and control strategy for grid-forming inverters to participate in frequency and voltage regulation in large grids, particularly focusing on transient and unbalance conditions. The strategy allows inverters with limited power adjustment capabilities, like electric vehicle chargers and curtailed solar plants, to contribute to grid stability [19].

M. Eggers et al. 2022, develops a current limitation strategy for grid-forming converters to handle deep voltage sags and phase angle jumps, which often cause synchronization issues. The proposed approach ensures voltage support and maintains synchronism across a wide range of grid frequencies and fault scenarios, improving the reliability of power electronic converters [20].

M. Eskandari and A. V. Savkin 2021, Fault ride-through (FRT) for IIDG units and its impact on transient stability. Current limiting during FRT affects transient stability of droop-based microgrids. Instability conditions explored via Lyapunov theory [21].

M. Ganjian Aboukheili et al. 2020, Control strategy for smooth transition in microgrids from grid-connected to islanding mode. Proposed linear voltage controller with capacitor current feedback ensures smooth transition and mitigates disturbances [22].

M. Li et al. 2021, Hierarchical control for smart and flexible microgrids. Three-level hierarchical control derived from ISA-95 standard enhances MGs' flexibility and operational efficiency [23].

N. M. Dehkordi and S. Z. Moussavi 2020, Secondary control for voltage and frequency in islanded microgrids with fault-tolerant communication networks. Adaptive consensus-based protocols improve reliability and resiliency against sensor and actuator faults [24].

N. Xue et al. 2023, focused on Strategies for achieving carbon neutrality through new energy technologies and finding out the Emphasis on green hydrogen and artificial carbon conversion technology to bridge new and fossil energy [25].

O. Ajala et al. 2023, focus on Model-order reduction and dynamic aggregation for GFM inverters and finding reduced-order models maintain current dynamics and significantly reduce computational costs [26].

P. H. Gadde and S. Brahma 2021, described control performance comparison of GFM and GFL inverters in unbalanced microgrids and focus on GFM inverters ensure better performance and stability under disturbances and faults [27].

P. M. Gajare et al. 2023, explained on Stable fault-ride-through behavior for GFM converters. Proposed adaptive inertia function improves fault recovery and resynchronization focused by authors [28].

S. D. Silva et al. 2023, focused on optimal ratio of GFM and GFL inverters for PEDG resiliency and finding out Analytical approach to determine optimal GFM/GFL ratio for stable and resilient power delivery [29].

S. Dedeoglu et al. 2021 & 2022, described nonlinear controllers for virtual inertia and current-limiting in VSCs and Improved nonlinear controllers ensure desired current limitation and system stability under grid faults [30-31].

T. Li et al. 2021 & Y. Jiang et al. 2022, focused on electrochemical advancements in zinc–air batteries and zinc-ion batteries and finding on bifunctional oxygen electrocatalysts and CuI cathodes enhance battery performance and cycle stability [32-33].

Y. Peng et al. 2020, focused on Luminescence mechanism in AIE materials and find the Multiscale computational approach elucidates aggregation effects on radiative and non-radiative decays [34].

Y. Zhang et al. 2023, described the Transient synchronization stability (TSS) analysis of GFM VSCs with current limitations and find the Current limitation causes significant deformation in power angle characteristics, posing challenges for TSS analysis [35].

Flow graph of the Methodology

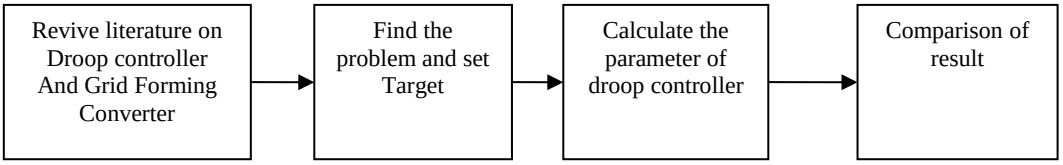

Figure 3.1 Flow graph of the Methodology

Through the use of input-to-state stability analysis, the inverter current's constant below-the-given value is analytically demonstrated [20,21]. By limiting the inverter current to a predetermined value, the universal robust droop controller preserves all of its benefits, including tight capacitor voltage management and constant protection for the inverter and filter. A set of guidelines for choosing the controller parameters and some remarks about it are also provided in order to finish the design process. Furthermore, it is demonstrated that the current-limiting characteristic is ensured regardless of changes in grid voltage and frequency, expanding the controller's application to scenarios involving grid failure. In contrast, a general control structure is suggested to accomplish droop control and current-limiting.

Power Quality Improvement

The PWM technique, switching, and nonlinear load all inevitably result in harmonic components in the inverter output voltage that deteriorate power quality. The inverter output filter is typically used to improve power quality, the inverter's output impedance should be carefully designed, and numerous control schemes have been put forth.

Inverter Output Filter

In order to remove harmonics and restore the desired voltage, a filter is frequently placed between the inverter and the load. As seen in Figure 3.2, LC and LCL filters are the most widely utilized passive inverter filters. Here, the inductor and capacitor's equivalent series resistances (ESR), which are often tiny values, are disregarded. The LCL filter is frequently used for grid-connected inverters, but the LC filter is commonly used for inverters with local loads.

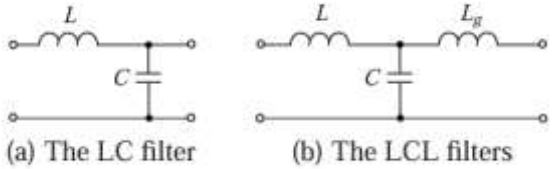

Figure 3.2 Circuit model of the passive power filter

The cut-off frequency fc of the LC filter is

$f_c = \frac{1}{2\pi\sqrt{LC}}$ Eqn. 3.1

The harmonics at frequencies higher than fc can be filtered out by it. But it creates a resonance that could result in a high load voltage thresold and enhance the harmonic current components at around fc. As a result, fc ought to be placed outside of the region occupied by the main current harmonic components. Usually, it can be

$\frac{f_{sw}}{3} \leq f_c \leq \frac{f_{sw}}{2}$ Eqn. 3.2

Design of Inverter Output Impedance

Because of the output filter inductor and/or the extremely inductive line impedance, the inverter output impedance is typically inductive. The line impedance in low-voltage applications is primarily resistive. It is simple to compel the output impedance to be resistive, resistive-inductive, or of another type because control techniques can be employed to change it. It has been noted that one significant factor in power sharing is the inverter output impedance. It would be intended to improve the power quality in this work.

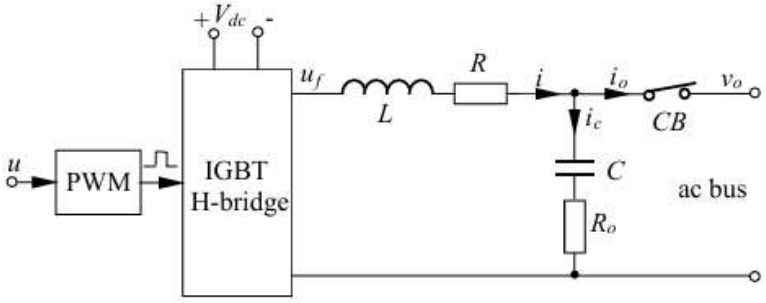

(a) Descriptive Circuit

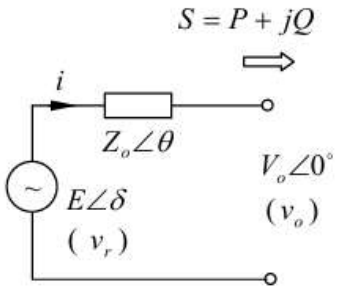

(b) Simplified model with terminal voltage v_o and terminal current i

Figure 3.3 A model of the single-phase inverter

The output impedance of an inverter is defined at the terminal with the load voltage v_o and the filter inductor current i, as illustrated in Figure 3.3(a). The inverter can therefore be modeled as the series connection of an output impedance (Zo) and a voltage reference (v_r), as seen in Figure 3.3(b). In other words, thinking of the filter capacitor as a component of the load As per Figure 3.3(a), disregarding the inductor's ESR,

$u_f = sLi + v_0$ Eqn. 3.3

Since the average of u_f over a switching period is approximately the same as u,

$v_r = u \approx sLi + v_0$ Eqn. 3.4

And $v_0 \approx v_r - Z_0(s)i$ Eqn. 3.5

With $Z_0(s) = sL$ Eqn. 3.6

where Zo(s) is the output impedance and v_r is the reference voltage. It is evident that in the absence of a controller, the output impedance Zo is inductive.

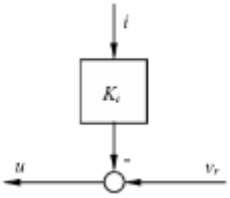

Figure 3.4 A controller to achieve the R-inverter

The control approach might be used to make the inverter output impedance resistive, as seen in Figure 3.4

According to Figure 3.4,

$u = v_r - K_i i$ Eqn. 3.7

Then, $v_r - K_i i \approx sLi + v_0$ Eqn. 3.8

Which gives the impedance Zo(s)

$Z_0(s) = K_i + sL$ Eqn. 3.9

This is the same as connecting the filter inductor L in series with a virtual resistor Ki. When Ki is large enough, the output impedance can be almost entirely resistive at the fundamental frequency, meaning that the inductor's sL impact is negligible.

$Z_0(s) \approx K_i$ Eqn. 3.10

If the effect of Ki is almost the same as the effect of the inductor sL, the output impedance would be resistive and inductive at the fundamental frequency, i.e., roughly

$Z_0(s) \approx K_i + sL$ Eqn. 3.11

Since the R-inverter's impedance is frequency-invariant and it is easier to correct for the impact of nonlinear loads, or harmonic current components, on the voltage threshold, it is arguably superior to the L-inverter. The inverter output impedance would be improved to lower the load voltage threshold by designing it to be capacitive.

Parallel Operation of Inverters

Droop control is a crucial technique for inverter parallel operation because it can maintain precise load sharing as well as good voltage and frequency regulation.

Conventional Droop Controller

An inverter can be modeled as a reference voltage source with an output impedance of Zo, as Figure 3.3(b) illustrates. Through the output impedance Zo, the real power P and reactive power Q are sent to the terminal.

$P = \left(\frac{EV_0}{Z_0} cos\delta - \frac{{V_0}^2}{Z_0}\right) cos\theta + \frac{EV_0}{Z_0} sin\delta \, sin\theta$ Eqn. 3.12

$Q = \left(\frac{EV_0}{Z_0} cos\delta - \frac{{V_0}^2}{Z_0}\right) sin\theta + \frac{EV_0}{Z_0} sin\delta \, cos\theta$ Eqn. 3.13

where Vo is the RMS value of the load voltage, E is the RMS value of the inverter source voltage, θ is the angle of the inverter output impedance, and δ is the phase difference between the supply and terminal.

For L-inverters, θ = 90◦. Then

$P = \frac{EV_0}{Z_0} sin\delta$ and

$Q = \frac{EV_0}{Z_0} cos\delta - \frac{{V_0}^2}{Z_0}$ Eqn.3.14

When δ is small,

$P\frac{EV_0}{Z_0} \approx \delta$ and $Q \approx \frac{E - V_0}{Z_0} V_0$ Eqn. 3.15

and roughly, P ∼ δ and Q ∼ Vo.

Hence, the conventional droop control strategy takes the form

$E = E^* - nQ$ Eqn. 3.16

$\omega = \omega^* - mP$ Eqn. 3.17

where E∗ is the rated RMS voltage of the inverter, ω∗ and ω are the rated and measured system line frequency, n and m are the droop coefficients. This strategy is shown in Figure 3.6(a).

For R-inverters, θ = 0◦. Then

$P = \frac{EV_0}{Z_0} cos\delta - \frac{{V_0}^2}{Z_0}$ and $Q = -\frac{EV_0}{Z_0} sin\delta$ Eqn. 3.18

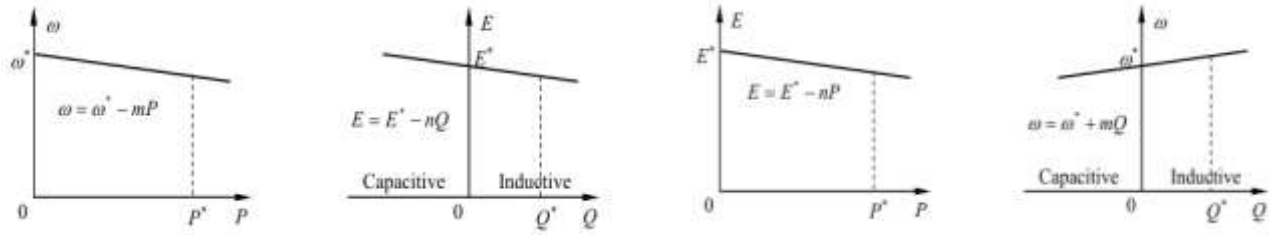

Figure 0.1 Droop controllers for the L-inverter and the R-inverter

When δ is small,

$P \approx \frac{E-V_0}{Z_0} V_0$ and $Q \approx -\frac{EV_0}{Z_0}\delta$ Eqn. 3.19

and, roughly, P ∼ Vo and Q ∼ −δ.

Hence, the conventional droop control strategy takes the form

$E = E^* - nP$ Eqn. 3.20

$\omega = \omega^* + mQ$ Eqn. 3.21

As seen in Figure 3.6(b). It is clear that the droop control technique differs for L and R inverters, and therefore C inverters would also have a distinct shape.

Current Limiting

The power is the control variable for the majority of droop controllers. Nevertheless, in the event of an abrupt load change or short circuit, the current remains unrestricted even with power control. Directly managing the active and reactive currents is one potential fix. The voltage difference between the grid voltage across the virtual complex impedance and the reference ac voltage sources was used to determine the active and reactive currents in. A technique presented in determined the reactive and active currents by calculating the reactive and active power.

Nevertheless, the ratio of the actual inverter output resistance to reactance is required for both of these techniques. Another approach described in employed the power angle of the load voltage and the amplitude and phase angle of the load current to determine the active and reactive currents.

Stability Analysis

After linearization around the equilibrium point, the small signal stability analysis may be used to determine the dynamic properties and stability of the parallel-operated inverter system. Using L-inverters and the traditional droop controllers (3.20) and (3.21), for instance, the linearized droop controller is when the power measurement block is near the equilibrium point.

$\Delta E(s) = -\frac{\omega_{fn}}{s+\omega_f}\Delta Q(s)$ Eqn. 3.22

$\Delta\omega(s) = -\frac{\omega_{fm}}{s+\omega_f}\Delta P(s)$ Eqn. 3.23

where ω_f is the cut-off frequency of the measuring filter. So in the time domain, these correlations are

$\Delta\dot{E} = -\omega_f \Delta E - \omega_f n \Delta Q$ Eqn. 3.24

$\Delta\dot{\omega} = -\omega_f \Delta\omega - \omega_f m \Delta P$ Eqn. 3.25

The characteristic equation for the entire system may then be found by combining the formulas for active and reactive power (3.12) and (3.13) with (3.24) and (3.25). The dynamic features and system stability could be examined using the characteristic equation as a basis.

Droop Controller without Voltage and Frequency Deviations

There is still a trade-off between power sharing and load voltage and frequency regulation when using a universal droop controller, even though it allows inverters with various output impedances to operate in parallel. Then, a query comes up: Is precise power sharing feasible in the absence of load voltage or frequency deviation?

A new droop controller that uses the transient droop characteristics and adopts the robust droop controller's structure is presented as a solution to this issue. This controller can maintain the nominal values of the load voltage and frequency while achieving proportional power sharing. This implies that an automatic compensation will be made for the voltage drop brought on by the inverter's output impedance. Additionally, no communication between parallel coupled inverters is required for this controller.

The Trade-off of the Droop Controller

The droop controller can take on several shapes depending on the sort of output impedance that inverters have. The analysis is made simpler by using the R-inverter as an example. It is simple to adapt the suggested droop controller to the L- and C-inverter cases.

The conventional droop controller of the R-inverter is

$E = E^* - nP$ Eqn. 3.26

$\omega = \omega^* - mQ$ Eqn. 3.27

The load voltage amplitude and frequency deviations brought on by the droop controller are −nP and mQ, respectively, based on equations (3.26) and (3.27). The variations are evidently present as long as the power is not zero. Furthermore, the load voltage amplitude deviation will increase due to the voltage drop across the inverter output impedance.

The Trade-off of the Robust Droop Controller

As the robust droop controller of the R-inverter is

$\dot{E} = K_e(E^* - V_0) - nP$ Eqn. 3.28

$\omega = \omega^* + mQ$ Eqn. 3.29

At the steady state, (3.28) becomes

$nP = K_e(E^* - V_0)$ Eqn. 3.30

According to (3.29) and (3.30), the deviations caused by the droop controller are $\frac{-nP}{K_e}$and mQ, respectively. Although by adjusting Ke, n and m, the deviations can be controlled to be small, they exist as long as the power is not zero.

The Droop Controller

The suggested droop controller uses the transient droop characteristics and takes on the robust droop controller's structure, as seen in Figure 3.7(a). This controller is quite basic, yet it works well:

$\dot{E} = K_e(E^* - V_0) - nP$ Eqn. 3.31

$\omega - \omega^* = m\tilde{Q}$ Eqn. 3.32

At steady state, there should be

$K_e(E^* - V_0) = n\tilde{P}$ Eqn. 3.33

Where

$\tilde{P} = H(s)P = \frac{\tau s}{\tau s+1}P$ Eqn. 3.34

$\tilde{Q} = H(s)Q = \frac{\tau s}{\tau s+1}Q$ Eqn. 3.35

Obviously, under the steady-state condition, both $\tilde{P}$ and $\tilde{Q}$ will be 0, thus the left-hand sides of (3.32) and (3.33) will also be 0. Hence, this yields

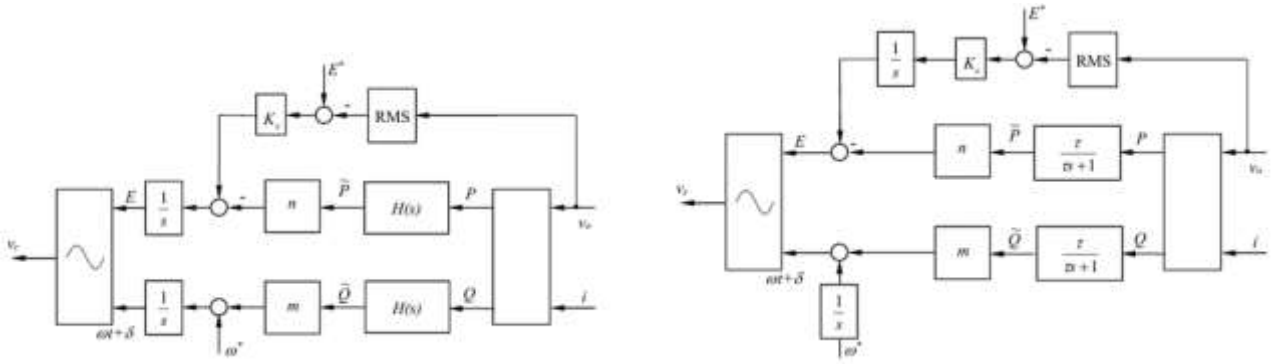

Figure 3.7 Robust droop controller and without zero-pole cancellation

$V_0 = E^*$ Eqn. 3.36

$\omega = \omega^*$ Eqn. 3.37

to ensure that there are no steady-state fluctuations in the magnitude or frequency of the load voltage. It shows that the automated compensation of the voltage drop on the inverter output impedance has taken place. There are two types of power sharing: reactive and active.

$P = \frac{1}{\tau s+1}\tilde{P}$ Eqn.3.38

$Q = \frac{1}{\tau s+1}\tilde{Q}$ Eqn. 3.39

When the initial conditions of both integral of $\tilde{P}$ and $\tilde{Q}$ are the same, it holds that

$P = \frac{1}{\tau}\int_0^{\infty}\tilde{P}dt + \tilde{P}$ Eqn. 3.40

$Q = \frac{1}{\tau}\int_0^{\infty}\tilde{Q}dt + \tilde{Q}$ Eqn. 3.41

As long as the transient active power $\tilde{P}$ and the transient reactive power $\tilde{Q}$ are proportionately shared—which can be accomplished by selecting appropriate n and m—the active power $\tilde{P}$ and reactive power $\tilde{Q}$ will be precisely proportionately shared, as per equations (3.40) and (3.41). But the system is intrinsically unstable due to the zero-pole cancellation brought on by the integrators and H(s).

Current Droop Controller

When a quick load shift or short circuit happens, currents are still unrestricted even if the power is managed. Direct regulation of the reactive and active currents is one potential remedy. It starts by creating a new current calculation unit that solely calculates the active and reactive currents based on the load voltage's angle.

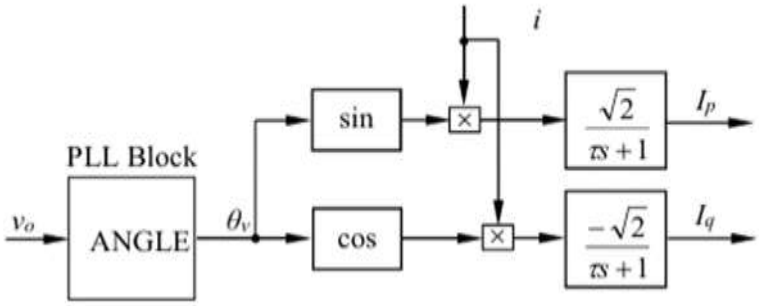

Figure 3.8 The current calculation unit

As shown in Figure 3.8, following applies

$I_p = \frac{\sqrt{2}}{\tau s+1} i\ sin\theta_v \approx Icos(\theta_v - \theta_i)$ Eqn.3.42

$I_q = \frac{-\sqrt{2}}{\tau s+1} i\ cos\theta_v \approx Isin(\theta_v - \theta_i)$ Eqn. 3.43

where θv is the angle of the inverter load voltage, θi is the inductor current's angle, and i is the inductor current. Keep in mind that this device only uses one Fourier block and requires the inverter load voltage angle v_o

Based on this current calculation unit, a current droop controller with robust form is proposed, which adopts the structure of the robust droop controller:

$\dot{E} = K_e(E^* - V_0) - nI_p$ Eqn. 3.44

$\omega = \omega^* + mI_q$ Eqn. 3.45

However, its current limiting ability is very weak. As shown in Figure 3.9, an adaptive coefficient is added to the voltage magnitude loop:

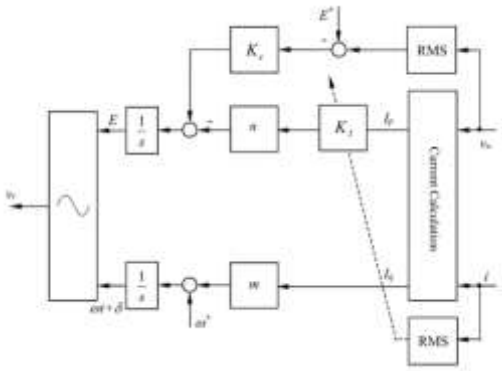

Figure 3.9 The current droop controller

$\dot{E} = K_e(E^* - V_0) - nK_II_p$ Eqn. 3.46

$\omega = \omega^* + mI_q$ Eqn. 3.47

Where

$K_I = (\frac{I}{I_r})^h$ Eqn. 3.48

And, h=1, 2, 3..

Here, n and m are set according to the voltage drop ratio R_v and frequency boost ratio R_f, with current I = Imax:

$n = \frac{K_e E^* R_v}{I_{max}}$ Eqn. 3.49

$m = \frac{\omega^* R_f}{I_{max}}$ Eqn. 3.50

Current Limiting

For conventional current droop controller, one has

$n = \frac{E^* R_v}{I_{max}}$ Eqn. 3.51

$m = \frac{\omega^* R_f}{I_{max}}$ Eqn. 3.52

According to (3.51) and (3.52), at the steady state, there should be

$I_p = \frac{E^* - E}{n} = \frac{E^* - E}{R_v E^*} I_{max}$ Eqn. 3.53

$I_q = \frac{\omega - \omega^*}{m} = \frac{\omega - \omega^*}{\omega^* R_f} I_{max}$ Eqn. 3.54

Assuming that $S^* = I_{max}E^*$, for robust droop controller, there are

$n = \frac{K_e R_v}{I_{max}}$ Eqn.3.55

$m = \frac{\omega^* R_f}{I_{max} E^*}$ Eqn. 3.56

According to (3.44), (3.45), (3.55) and (3.56), at the steady state, there should be

$I_p = \frac{K_e(E^* - V_0)}{nV_0} = \frac{E^* - V_0}{R_v V_0} I_{max}$ Eqn. 3.57

$I_q = \frac{\omega - \omega^*}{mV_0} = \frac{(\omega - \omega^*)}{\omega^* R_f V_0} I_{max}$ Eqn. 3.58

According to (3.46), (3.47), (3.49) and (3.50), at the steady state, there should be

$I_p = \frac{K_e(E^* - V_0)}{nK_I} = \frac{K_e I_{max}(E^* - V_0)}{K_e R_v E^* K_I} = \frac{(E^* - V_0)}{R_v E^* K_I} I_{max}$ Eqn. 3.59

$I_q = \frac{\omega - \omega^*}{m} = \frac{(\omega - \omega^*)}{\omega^* R_f} I_{max}$ Eqn.3.60

Ignoring the voltage drop on the inverter output impedance, then Vo ≈E. When the inverter is working at the rated current I = Ir, there will be KI = 1 and Vo ≈ E∗. Then

$I_p = \frac{(E^* - V_0)}{R_v E^*} I_{max} \approx \frac{(E^* - E)}{R_v E^*} I_{max} \approx \frac{(E^* - V_0)}{R_v V_0} I_{max}$ Eqn. 3.61

This indicates that when the inverter is working at the rated current, the active current of the proposed CDC is almost the same with the ones of the conventional current droop controller and the robust droop controller. When the inverter is working above the rated current I > I_r, there will be KI > 1 and V_o < E∗. Then

$I_p < \frac{(E^* - V_0)}{R_v E^*} I_{max} \approx \frac{(E^* - E)}{R_v E^*} I_{max} < \frac{(E^* - V_0)}{R_v V_0} I_{max}$ Eqn. 3.62

Thus, I_p with the proposed CDC is better limited than the ones with the conventional current droop controller and the robust droop controller. The bigger the current I, the stronger the limitation on I_p. Similarly, K_I can be used in the I_q droop to limit the reactive current.

Power Sharing

In this, h is chosen to be 2 as an example: h=2,

According to (3.42) and (3.43), there is

$I^2 = {I_p}^2 + {I_q}^2$ Eqn. 3.63

According to (3.46), there is

$K_e(E^* - V_0) = n(\frac{I}{I_r})^2 I_p$ Eqn. 3.64

By solving (3.47), (3.63) and (3.64), one gets

$I_q = \frac{\omega - \omega^*}{m}$ Eqn.3.65

When two inverters are operated in parallel,

$\frac{I_{p1}}{I_{p2}} = \frac{I_{q1}}{I_{q2}} = \frac{1}{N}$ Eqn. 3.66

$$I_p = \frac{3\left(\sqrt{\frac{P^4 K_p^2 E^{*2}}{4\pi^2} + \frac{(\omega-\omega^*)^6}{27m^6}} + \frac{P^2 K_p E^*}{2\pi}\right)^{2/3} - \left(\frac{\omega-\omega^*}{m}\right)^2}{3\left(\sqrt{\frac{P^4 K_p^2 E^{*2}}{4\pi^2} + \frac{(\omega-\omega^*)^6}{27m^6}} + \frac{P^2 K_p E^*}{2\pi}\right)^{1/3}} \qquad I_q = \frac{\omega - \omega^*}{m}$$

which guarantees the current sharing of the parallel operated inverters. Especially, when the short-circuit happens, there will be $V_o = 0$ and

Obviously, the current sharing is also guaranteed when the short-circuit happens.

Result and Discussion

The MATLAB/Simulink simulations and studies that focus on different ways to preserve system stability under varying settings are summarized in table 1. For every study given, the result is "System operation stable," meaning that the system remained stable under the evaluated conditions.

Table 1 Summary of previous work

Reference	Platform	Method	Outcome
[1]	MATLAB/Simulink	Current limiting and stability	System operation stable
[3]	MATLAB/Simulink	Constant Power load and stability	System operation stable
[4]	MATLAB/Simulink	Current and Power limiting with stability	System operation stable
[10]	MATLAB/Simulink	Power Sharing in an Islanded AC Microgrid Using Modified Reverse Droop Control Strategy	System operation stable
[12]	MATLAB/Simulink	Fault Modeling of Droop-Controlled IIDG and Its Cluster	System operation stable
[19]	MATLAB/Simulink	Grid-Forming Nature Retaining Fault Ride-Through Control	System operation stable

Conclusion

The study's outline includes the calculation of droop controller with current and power limiting. In addition, achieving stable system operation under these circumstances is the goal of this suggested study.

References

[1] A. C. Braitor, G. C. Konstantopoulos and V. Kadirkamanathan, "Current-Limiting Droop Control Design and Stability Analysis for Paralleled Boost Converters in DC Microgrids," in IEEE Transactions on Control Systems Technology, vol. 29, no. 1, pp. 385-394, January 2021, doi: 10.1109/TCST.2019.2951092.

[2] A. G. Paspatis, G. C. Konstantopoulos and J. M. Guerrero, "Enhanced Current-Limiting Droop Controller for Grid-Connected Inverters to Guarantee Stability and Maximize Power Injection Under Grid Faults," in IEEE Transactions on Control Systems Technology, vol. 29, no. 2, pp. 841-849, March 2021, doi: 10.1109/TCST.2019.2955920.

[3] A. K. Gupta, K. M. P and R. Batra, "Use of Different Control Strategies to Design Converters and Inverters for Sustainable Grids," 2023 International Conference on Power Energy, Environment & Intelligent Control (PEEIC), Greater Noida, India, pp. 1148-1153, 2023. doi: 10.1109/PEEIC59336.2023.10451471.

[4] A. Saleh, A. Rastegarnia, A. Farzamnia and K. T. T. Kin, "Power and Current Limiting Strategy Based on Droop Controller with Floating Characteristic for Grid-Connected Distributed Generations," in IEEE Access, vol. 10, pp. 13966-13973, 2022. (Cross Reference)

[5] A. Zapata, D. Santos, D. Wu and D. Rodríguez, "High Penetration of Inverter Based Resources Assessment on Stability and System Strength," IEEE Power & Energy Society General Meeting (PESGM), Orlando, FL, USA, pp. 1-5, 2023. doi: 10.1109/PESGM52003.2023.10252759.

[6] Al-Saadi, M., Al-Greer, M. Short, M. "Strategies for Controlling Micro grid Networks with Energy Storage Systems: A Review," Energies 2021.

[7] B. Mishra and M. Pattnaik, "Enhancement of Power Sharing in an Islanded AC Microgrid Using Modified Reverse Droop Control Strategy," IEEE 3rd International Conference on Smart Technologies for Power, Energy and Control (STPEC), Bhubaneswar, India, pp. 1-6, 2023. doi: 10.1109/STPEC59253.2023.10430624.

[8] C. Bisht and P. Kundu, "Fault Recovery of Grid-Forming Inverter by Droop Coefficient Modifier," IEEE 3rd International Conference on Smart Technologies for Power, Energy and Control (STPEC), Bhubaneswar, India, pp. 1-6, 2023. doi: 10.1109/STPEC59253.2023.10431305.

[9] C. Fang and L. Mu, "Analytical Fault Modeling of Droop-Controlled IIDG and Its Cluster," in IEEE Transactions on Smart Grid, 2024.

[10] D. Çelik and M. E. Meral, "A flexible control strategy with overcurrent limitation in distributed generation systems," Int. J. Electr. Power Energy Syst., vol. 104, pp. 456-471, January 2019.

[11] D. Yan, J. Benzaquen and D. Divan, "Transient Stability Comparison of Grid-Forming and Grid-Following Inverter-Based Resources," 2024 IEEE Texas Power and Energy Conference (TPEC), College Station, TX, USA, pp. 1-6, 2024. doi: 10.1109/TPEC60005.2024.10472263.

[12] Dedeoglu and G. C. Konstantopoulos, "Avoiding Circulating Current via Current-Limiting Control in AC Microgrids with Parallel Three-Phase Inverters," IECON 47th Annual Conference of the IEEE Industrial Electronics Society, Toronto, Canada, pp. 1-6, 2021.

[13] J. Liu, C. Zhao and Z. Xie, "Power and Current Limiting Control of Wind Turbines Based on PMSG under Unbalanced Grid Voltage," in IEEE Access, vol. 9, pp. 9873-9883, 2021. doi: 10.1109/ACCESS.2021.3049839.

[14] K. Yamanokuchi, H. Watanabe and J. -I. Itoh, "Distributed Control Method for Power Conversion System with Series-Connected Autonomous Modular Converters," in IEEE Transactions on Power Electronics, vol. 38, no. 12, pp. 15242-15252, December 2023. doi: 10.1109/TPEL.2023.3304417.

[15] L. Zhou, A. Swain, and A. Ukil, "Reinforcement learning controllers for enhancement of low voltage ride through capability in hybrid power systems," IEEE Trans. Ind. Informat., vol. 16, no. 8, pp. 5023-5031, August 2020.

[16] M. A. Awal, M. R. K. Rachi, H. Yu, S. Schroder, J. Dannehl and I. Husain, "Grid-Forming Nature Retaining Fault Ride-Through Control," IEEE Applied Power Electronics Conference and Exposition (APEC), Orlando, FL, USA, pp. 2753-2758, 2023. doi: 10.1109/APEC43580.2023.

[17] M. E. Meral and D. Çelík, "A comprehensive survey on control strategies of distributed generation power systems under normal and abnormal conditions," Annu. Rev. Control, vol. 47, pp. 112-132, January 2019.

[18] M. E. Meral and D. Çelik, "Proportional complex integral based control of distributed energy converters connected to unbalanced grid system," Control Eng. Pract., vol. 103, pp. 1-13, October 2020.

[19] M. Eggers, H. Yang, H. Just and S. Dieckerhoff, "Virtual-Impedance-Based Droop Control for Grid-Forming Inverters with Fast Response to Unbalanced Grid Faults," IEEE 11th International Symposium on Power Electronics for Distributed Generation Systems (PEDG), Dubrovnik, Croatia, pp. 122-129, 2020.

[20] M. Eggers, P. Teske and S. Dieckerhoff, "Virtual-Impedance-Based Current-Limitation of Grid-Forming Converters for Balanced and Unbalanced Voltage Sags," IEEE 13th International Symposium on Power Electronics for Distributed Generation Systems (PEDG), Kiel, Germany, pp. 1-6, 2022.

[21] M. Eskandari and A. V. Savkin, "on the impact of fault ride-through on transient stability of autonomous microgrids: Nonlinear analysis and solution," IEEE Trans. Smart Grid, vol. 12, no. 2, pp. 999-1010, March 2021.

[22] M. Ganjian-Aboukheili, M. Shahabi, Q. Shafiee, and J. M. Guerrero, "Seamless transition of microgrids operation from grid-connected to islanded mode," IEEE Trans. Smart Grid, vol. 11, no. 3, pp. 2106-2114, May 2020.

[23] M. Li, Y. Gui, Y. Guan, J. Matas, J. M. Guerrero and J. C. Vasquez, "Inverter Parallelization for an Islanded Microgrid Using the Hopf Oscillator Controller Approach with Self-Synchronization Capabilities," in IEEE Transactions on Industrial Electronics, vol. 68, no. 11, pp. 10879-10889, November 2021.

[24] N. M. Dehkordi and S. Z. Moussavi, "Distributed resilient adaptive control of islanded microgrids under sensor/actuator faults," IEEE Trans. Smart Grid, vol. 11, no. 3, pp. 2699-2708, May 2020.

[25] N. Xue, X. Wu, U. Muenz, N. Benesch and H. Electric, "Grid-Forming Control Benchmarking for 100% Inverter-Based Systems: Case Study on Hawai i Island," 2023 IEEE Power & Energy Society General Meeting (PESGM), Orlando, FL, USA, pp. 1-5, 2023.

[26] O. Ajala, N. Baeckeland, B. Johnson, S. Dhople and A. Domínguez-Garcia, "Model Reduction and Dynamic Aggregation of Grid-Forming Inverter Networks," in IEEE Transactions on Power Systems, vol. 38, no. 6, pp. 5475-5490, November 2023.

[27] P. H. Gadde and S. Brahma, "Comparison of PR and PI Controllers for Inverter Control in an Unbalanced Microgrid," 52nd North American Power Symposium (NAPS), Tempe, AZ, USA, pp. 1-6, 2021.

[28] P. M. Gajare, M. Miranbeigi, J. Benzaquen and D. Divan, "On the Fault-Ride-Through Dynamics of Grid-Forming Converters-A Multi-dimensional Adaptive Inertia Approach," IEEE Applied Power Electronics Conference and Exposition (APEC), Orlando, FL, USA, pp. 1489-1495, 2023.

[29] S. D'silva, M. Hosseinzadehtaher, A. Zare, M. B. Shadmand, S. Bayhan and H. Abu-Rub, "ANN-based Cooperative Frequency Restoration in a Network of Grid-forming and Grid-following Inverters," IEEE Energy Conversion Congress and Exposition (ECCE), Nashville, TN, USA, pp. 1453-1460, 2023.

[30] S. Dedeoglu, G. C. Konstantopoulos and H. Komurcugil, "Current-Limiting VSG for Renewable Energy Applications," IEEE 30th International Symposium on Industrial Electronics (ISIE), Kyoto, Japan, pp. 01-05, 2021.

[31] S. Dedeoglu, G. C. Konstantopoulos and H. Komurcugil, "Current-Limiting Virtual Synchronous Control and Stability Analysis Considering DC-Link Dynamics Under Normal and Faulty Grid Conditions," in IEEE Journal of Emerging and Selected Topics in Power Electronics, vol. 10, no. 2, pp. 2516-2527, April 2022.

[32] T. Li, Y. Li, S. Li and W. Zhang, "Research on Current-Limiting Control Strategy Suitable for Ground Faults in AC Microgrid," in IEEE Journal of Emerging and Selected Topics in Power Electronics, vol. 9, no. 2, pp. 1736-1750, April 2021.

[33] Y. Jiang, X. Li, C. Qin, X. Xing, and Z. Chen, "Improved particle swarm optimization based selective harmonic elimination and neutral point balance control for three-level inverter in low-voltage ride-through operation," IEEE Trans. Ind. Informat., vol. 18, no. 1, pp. 642-652, Jan. 2022.

[34] Y. Peng, Z. Shuai, X. Liu, Z. Li, J. M. Guerrero, and Z. J. Shen, "Modeling and stability analysis of inverter-based microgrid under harmonic conditions," IEEE Trans. Smart Grid, vol. 11, no. 2, pp. 1330-1342, Mar. 2020.

[35] Y. Zhang, C. Zhang, R. Yang, M. Molinas and X. Cai, "Current-Constrained Power-Angle Characterization Method for Transient Stability Analysis of Grid-Forming Voltage Source Converters," in IEEE Transactions on Energy Conversion, vol. 38, no. 2, pp. 1338-1349, June 2023.

[36] https://in.mathworks.com/discovery/droop-control.html